Appl. Phys. B 68, 713–718 (1999) / DOI 10.1007/s003409901394

Applied Physics B
Lasers
and Optics

Sum-frequency vibrational spectroscopy of a monolayer self-assembled on gold: interference between resonant and nonresonant contributions of nonlinear polarization

Yoshihito Tanaka[1,*], **S. Lin**[1,**], **M. Aono**[1,2], **T. Suzuki**[1]

[1] The Institute of Physical and Chemical Research (RIKEN), 2-1 Hirosawa, Wako, Saitama 351-0198, Japan
[2] Department of Precision Science and Technology, Osaka University, Osaka, Japan

Received: 21 August 1998/Revised version: 16 September 1998/Published online: 24 February 1999

Abstract. The spectral profiles of sum-frequency signal from CH vibrational modes of octadecanethiol (ODT) self-assembled on gold have been studied for several optical configurations of incident beams. The observed spectra, generally of the shape of dispersion type, have been interpreted by the interference between the resonant contribution from the CH stretching modes of adsorbed molecules and the nonresonant contribution from the gold substrate. We have shown for the first time that the contribution from the *zzz* component of the resonant nonlinear susceptibility $\chi^{(R)}_{zzz}$ is dominant in the observed resonant signals, whereas all of the *ijk* components contribute to the nonresonant signal. The transition frequencies and the relative amplitude of resonant signals are also determined for the CH_3 vibrational modes of ODT on gold.

PACS: 42.65; 78.65

Regularly arranged molecules on surfaces have recently been investigated intensively using the sum-frequency generation (SFG) technique. The sum-frequency (SF) vibrational spectroscopy of Langmuir–Blodgett (LB) films on a solid substrate, liquid–air interface of methanol, and hydrogen adsorbed on a crystal have been reported in the last decade [1–7]. In SF vibrational spectroscopy, the samples are irradiated by a tunable mid-infrared (MIR) beam and a fixed-frequency visible (VIS) beam. The SF signal is enhanced when the MIR frequency resonates with a vibrational mode of surface species. This technique has the following advantages when applied to the regularly arranged adsorbates on surfaces. First, the SF spectroscopic method is only sensitive, within the electric dipole approximation, to those surface species without inversion symmetry. Second, the infrared spectroscopic information is upconverted to the visible by the sum-frequency generation process, thus enabling a high sensitive detection with a photomultiplier tube. Furthermore, since this technique is vibrational-mode selective, the relative signal intensity of vibrational modes provides information on the molecular orientation [8–11]. In addition, it is possible to make an ultrafast time-resolved measurement by employing a pulsed laser of short duration [12–16].

When the SF spectroscopic technique is applied to molecules on certain metals, a large SF signal from the metal surface of a nonresonant type [17–19] has to be taken into account to extract a true picture of vibrationally resonant modes of adspecies. The nonresonant signal modifies the spectral profile through the interference between vibrationally resonant and nonresonant components of nonlinear polarization. It will be possible, however, through a proper analysis of the interference to extract directly the information on the phase relation among the vibrational modes, which are related to the polar orientation of the atomic group [20]. The relative phase between vibrationally resonant modes has been determined by using an external reference [20–22] and by utilizing the interfering adjacent vibrational modes [9, 10]. Self-assembled monolayer (SAM) on gold is of considerable attention recently for both technological and fundamental reasons [23]. In SF spectroscopy of SAM, the signal of phase additive between the resonant and nonresonant components has been reported in the counterpropagating configuration of two incident beams [17, 18]. The SF signal of phase destructive has also been reported for a layer of inverted molecules on gold [18]. The phase angle, however, has not been fully analyzed yet.

In this paper, SF signals from SAM on gold observed in the various configurations of incident beams are studied. Every component of the nonlinear susceptibility has been estimated through the analysis of the spectral line profiles.

1 Experimental

The MIR pulses tunable across the CH vibrational frequencies of SAM in the 3–4 μm range were provided from an optical parametric amplifier (OPA) using a $MgO:LiNbO_3$ crystal.

* *Present address*: Harima RIKEN, 323-3 Mikazuki, Sayo-gun, Hyogo, 679-5143, Japan
(Fax: +81-7915/8-2810, E-mail: yotanaka@postman.riken.go.jp)
** On leave from Fujian Institute of Research on the Structure of Matter, Chinese Academy of Sciences, Fuzhou, Fujian 350002, China

This OPA has been described in detail elsewhere [24], and is only briefly outlined here (see Fig. 1).

The OPA system generating the tunable MIR pulses is composed of a 7% MgO-doped $LiNbO_3$ crystal using a 2 ps Ti:sapphire laser as a pump source and a synchronous optical parametric oscillator (OPO) as a seeding source. The Ti:sapphire laser (Spectra-Physics, Tsunami, picosecond version) is amplified by a home-made regenerative amplifier [25] to produce 10-Hz pulses tunable between 750 and 840 nm with a pulse duration of 2.0 ps and a bandwidth of 8 cm^{-1}. In this experiment, the Ti:sapphire laser at a fixed wavelength of 810 nm with a pulse energy of 500 μJ was used for OPA. The seeding OPO laser is a commercial one (Spectra-Physics, MOPO730) pumped by the third harmonics of a Q-switched YAG laser, which delivers pulses with a tunability in the 0.42–1.7 μm range, a pulse duration ≈ 3 ns, a pulse energy between 5 and 80 mJ, and a bandwidth < 0.2 cm^{-1} (FWHM). A pulse energy ≈ 1 mJ was used for seeding the present OPA. Scanning of the MIR wavelength is accomplished by simply changing the seeding wavelength. In the wavelength range from 3.2 to 3.6 μm, a pulse energy of 15 μJ was uniformly obtained at a fixed crystal angle with a negligible beam walk-off in the present SFG experiment. The output MIR pulse had a bandwidth < 10 cm^{-1} and a pulse duration ≈ 3 ps, which were primarily determined by the characteristics of the Ti:sapphire laser. Such a short pulse duration is not essentially needed for the spectroscopic measurement. It may, however, have an advantage in the sample damage threshold [7]. The pulse-to-pulse energy fluctuation of the obtained MIR beam was around 10%.

The sample consisted of a monolayer of octadecanethiol (ODT) ($CH_3(CH_2)_{17}SH$) on an evaporated gold film with a thickness of 200 nm. The gold film evaporated on a glass plate was immersed in dilute (≈ 0.5 mM) ODT solutions of ethanol for several hours. After the immersion, the sample was rinsed with absolute ethanol to remove the residual adsorbate and solvent. This ODT sample has been stable for a few months.

The SFG experiments were carried out with the sample in air at room temperature in the various optical configurations of the incident beams. The VIS beam energy of 100 μJ was a part of the Ti:sapphire pulse divided by a beam splitter. The VIS and MIR pulses were focused onto the sample surface to a beam waist of 300 and 150 μm, respectively. The spatial overlap and temporal coincidence were first carried out by using a GaAs plate as a reference sample taking advantage of the large nonlinear susceptibility (around 10 times higher than that of the ODT/gold). Then, GaAs was replaced by the ODT sample for the final adjustment of the SFG signal. All of the polarization planes were chosen to be parallel to the plane of incidence. The sum-frequency signal, being passed through a short-wavelength-pass filter, a polarizer, and a monochromator, was detected by a photomultiplier tube (PMT). The signal was then averaged over 100 pulses by a gated integrator (SR250) and was stored in a personal computer. The scanning speed of the MIR frequency was about 0.17 cm^{-1}/s.

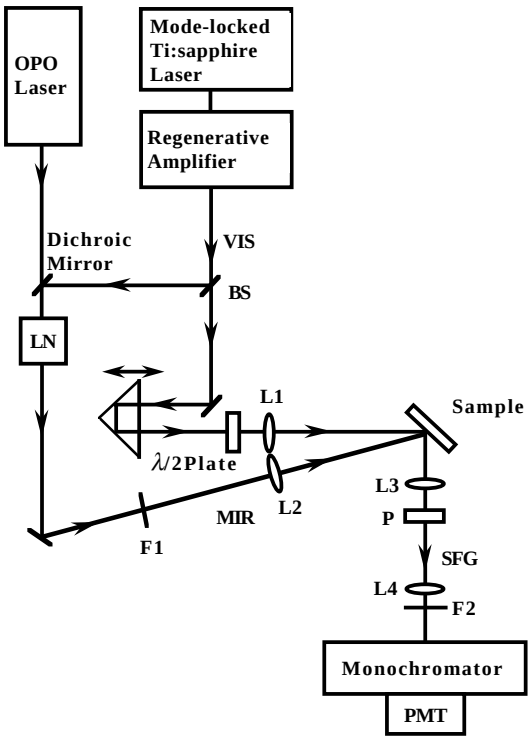

Fig. 1. Schematic diagram of experimental setup in the co-propagating configuration. The mid-infrared (MIR) beam generated in a 7% MgO:$LiNbO_3$ (LN) crystal and the visible (VIS) beam from a beam splitter (BS) are focused with the lenses (L1, L2) onto the sample. Ge filter (F1) is used to block the residual visible beam. The SF signal passed through the lenses (L3, L4), an analyzer (P), a short-wavelength-pass filter (F2), and a monochromator, is observed with photomultiplier tube (PMT)

2 Results

The optical configurations of the incident and SF beams in the present measurement are sketched in Fig. 2. The incidence angles of the visible and MIR beams are denoted by θ_{VIS} and θ_{MIR}, respectively. The number of the maximum SF photons observed in the co-propagating configuration shown in Fig. 2a is about 12 photons for each pulse, which corresponds to the quantum conversion efficiency of around 2×10^{-14}.

The SF spectra shown in Fig. 3a–d were obtained in the configuration of Fig. 2a–d, respectively. Normalization of the SF spectra against the MIR power was not necessary because of the constant MIR power during the measurement. Three resonant SF signals are seen in Fig. 3a. The peaks around

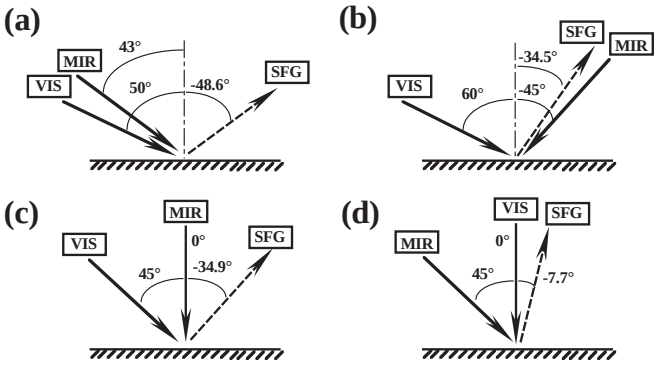

Fig. 2a–d. Sketch of the SFG configuration **a** $\theta_{VIS} = 50°$, $\theta_{MIR} = 43°$. **b** $\theta_{VIS} = 60°$, $\theta_{MIR} = -45°$. **c** $\theta_{VIS} = 45°$, $\theta_{MIR} = 0°$. **d** $\theta_{VIS} = 0°$, $\theta_{MIR} = 45°$. VIS, MIR, and SFG represent the visible beam, the mid-infrared beam, and the SF signal, respectively

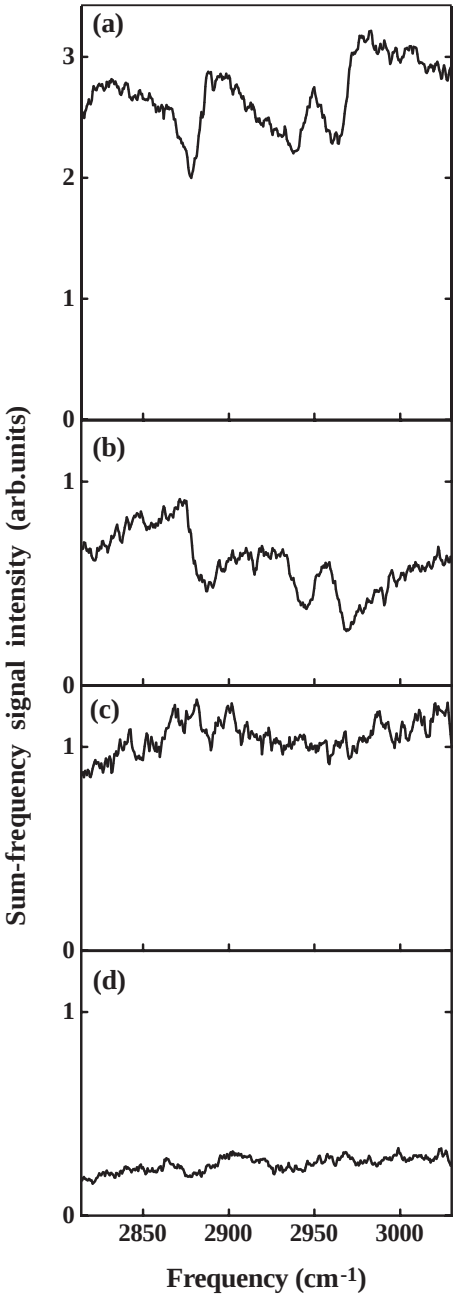

Fig. 3. SF spectra of a monolayer of octadecanethiol self-assembled on gold corresponding to the optical configurations shown in Fig. 2

2880 cm^{-1}, 2938 cm^{-1}, and 2966 cm^{-1} are assigned as the symmetric CH stretching mode of the CH_3 group, the overtone of the methyl HCH deformation mode, which acquires intensity through Fermi resonance with the symmetric CH stretching mode, and the degenerate CH stretching mode of the CH_3 group, respectively [5]. For the counterpropagating configuration with $\theta_{\mathrm{VIS}} = 60°$ and $\theta_{\mathrm{MIR}} = -45°$, the resonant SF signals of a dispersion type are also clearly seen in Fig. 3b. On the other hand, we do not find any clear resonant signal of vibrational mode in the SF spectra for the configurations of ($\theta_{\mathrm{VIS}} = 45°$, $\theta_{\mathrm{MIR}} = 0°$) and ($\theta_{\mathrm{VIS}} = 0°$, $\theta_{\mathrm{MIR}} = 45°$) as shown in Fig. 3c,d.

In the configurations (a) and (b), the SF signal intensity from a clean gold film evaporated on a glass plate was also measured. The intensity of the nonresonant SFG signal from ODT/gold in the configurations (a) and (b), was around 60(±10)% and 110(±20)%, respectively, of that for a clean gold film. We also made an SFG experiment for an LB film of ODT on a glass plate, and obtained no detectable nonresonant SF signal from this sample.

In the present SFG measurement, the signal intensity was observed to be independent of the azimuthal angle, suggesting an azimuthal isotropy of ODT/gold.

3 Analysis and discussions

3.1 Theoretical background

The SF signal originates from the nonlinear polarization $P^{(2)}$ induced by the electric fields of VIS and MIR beams. The i-component $P_i^{(2)}$ is expressed as [26],

$$P_i^{(2)} = \sum_{j,k} C(ijk)\chi_{ijk}^{(2)} E^{\mathrm{VIS}} E^{\mathrm{MIR}}, \tag{1}$$

with

$$C(ijk) = e_i F^{ii} e_j F^{jj} e_k F^{kk}, \tag{2}$$

where i, j, and k denote the Cartesian coordinates, and $\chi_{ijk}^{(2)}$ is the ijk component of the macroscopic nonlinear susceptibility tensor. E^{VIS} and E^{MIR} are the amplitude of electric fields of VIS and MIR beams, respectively. e_i, e_j, and e_k are the i, j, and k component of the SF, VIS, and MIR unit polarization vectors, respectively. F^{ii} represents the i component of the Fresnel factor [27–29]. $\chi_{ijk}^{(2)}$ is expressed as a superposition of resonant contributions of the ν-th vibrational mode $\chi_{ijk,\nu}^{(\mathrm{R})}$ and a nonresonant contribution $\chi_{ijk}^{(\mathrm{NR})}$:

$$\chi_{ijk}^{(2)} = \chi_{ijk}^{(\mathrm{NR})} + \sum_{\nu} \chi_{ijk,\nu}^{(\mathrm{R})}(\omega), \tag{3}$$

with

$$\chi_{ijk,\nu}^{(\mathrm{R})}(\omega) = \frac{A_{ijk,\nu}}{\omega - \omega_\nu + \mathrm{i}\Gamma_\nu}, \tag{4}$$

where ω_ν, $A_{ijk,\nu}$, Γ_ν and ω are the transition frequency, the amplitude, the damping constant of the ν-th resonant vibration, and the MIR beam frequency, respectively. Substituting (3) and (4) into (1), we obtain the p-polarization component $P_{\mathrm{p}}^{(2)}$ induced by the irradiation of both p-polarized VIS and MIR beams, as,

$$P_{\mathrm{p}}^{(2)} = \left(\sum_{i,j,k} C(ijk)\chi_{ijk}^{(\mathrm{NR})} + \sum_{i,j,k} C(ijk) \sum_{\nu} \frac{A_{ijk,\nu}}{\omega - \omega_\nu + \mathrm{i}\Gamma_\nu} \right) \times E^{\mathrm{VIS}} E^{\mathrm{MIR}}. \tag{5}$$

Here, the surface normal is chosen along the z axis with the plane of incidence in the xz plane. In the case of a boundary between isotropic media, $\chi_{ijk}^{(2)}$ is reduced to four nonvanishing components, designated by $\chi_{xzx}^{(2)}$, $\chi_{zxx}^{(2)}$, $\chi_{zzz}^{(2)}$, and $\chi_{xxz}^{(2)}$. When

the SF frequency and the VIS frequency are both far from resonance, the relation $\chi^{(2)}_{xzx} = \chi^{(2)}_{zxx}$ is also derived.

The nonresonant part of nonlinear susceptibility $\chi^{(\mathrm{NR})}_{ijk}$ can generally be written as [30]

$$\chi^{(\mathrm{NR})}_{ijk} = \chi^{(\mathrm{NR})}_{ijk,\mathrm{s}} + \chi^{(\mathrm{NR})}_{ijk,\mathrm{a}} + \chi^{(\mathrm{NR})}_{ijk,\mathrm{s-a}}\,, \tag{6}$$

where s, a, and s–a denote the contributions from the substrate, the adsorbate, and the adsorbate–substrate interaction, respectively.

The coefficients $C(ijk)$ are calculated based on the phenomenological method developed by Mizrahi et al. [29], and are shown in Table 1. In the present calculation of Fresnel factors, it is assumed (or defined) that the nonlinear polarization is induced by the fields in the substrate just beneath the thin layer (not inside the thin layer). The refractive indices of gold for VIS, MIR, and SFG frequencies used in our calculation are 0.17–4.86 i, 2.05–21.33 i, and 0.17–3.15 i, respectively [31].

3.2 Resonant SF signals

As seen in Table 1 $C^{(\mathrm{c})}(zzz)$ and $C^{(\mathrm{c})}(xxz)$ are zero for ($\theta_{\mathrm{VIS}} = 45°$, $\theta_{\mathrm{MIR}} = 0°$), and $C^{(\mathrm{d})}(xzx)$ and $C^{(\mathrm{d})}(zzz)$ are zero for ($\theta_{\mathrm{VIS}} = 0°$, $\theta_{\mathrm{MIR}} = 45°$), because the z component of one of the unit polarization vectors is zero. Here, superscript (n) is used to represent the corresponding configuration depicted in Fig. 2. Since no clear resonant signal was observed in Fig. 3c, the contribution of $(C^{(\mathrm{c})}(xzx)\chi^{(\mathrm{R})}_{xzx} + C^{(\mathrm{c})}(zxx)\chi^{(\mathrm{R})}_{zxx})$ $(= (C^{(\mathrm{c})}(xzx) + C^{(\mathrm{c})}(xzx))\chi^{(\mathrm{R})}_{xzx})$ term to the resonant signal is negligible. Similarly, $C^{(\mathrm{d})}(xxz)\chi^{(\mathrm{R})}_{xxz}$ is also negligible as seen from Fig. 3d. Thus, we conclude that the resonant SF signal is dominantly characterized by $\chi^{(\mathrm{R})}_{zzz}$.

The contribution of $\chi^{(\mathrm{R})}_{zzz}$ to the resonant signals can be estimated from Fig. 3 and Table 1 as follows: The resonant SF signal intensity in Fig. 3a is more than 7 and 10 times larger than that in Fig. 3c and d, respectively. If $\left|\sum_{i,j,k} C(ijk)\chi^{(\mathrm{NR})}_{ijk}\right| > \left|\sum_{i,j,k} C(ijk)\chi^{(\mathrm{R})}_{ijk}\right|$, which is actually satisfied in the present experimental results, the resonant signal intensity is approximately proportional to $\left|\sum_{i,j,k} C(ijk)\chi^{(\mathrm{R})}_{ijk}\right|$. This gives

$$\begin{aligned}\left|\sum_{i,j,k} C^{(\mathrm{a})}(ijk)\chi^{(\mathrm{R})}_{ijk}\right| &\gg 7\left|(C^{(\mathrm{c})}(xzx) + C^{(\mathrm{c})}(zxx))\chi^{(\mathrm{R})}_{xzx}\right| \\ &\approx 10\left|C^{(\mathrm{d})}(zxx)\chi^{(\mathrm{R})}_{zxx} + C^{(\mathrm{d})}(xxz)\chi^{(\mathrm{R})}_{xxz}\right|\,.\end{aligned} \tag{7}$$

After some algebraic manipulations, the following relation is obtained for the configuration (a):

$$\begin{aligned}\left|C^{(\mathrm{a})}(zzz)\chi^{(\mathrm{R})}_{zzz}\right| &\gg 2.8\left|(C^{(\mathrm{a})}(xzx) + C^{(\mathrm{a})}(zxx))\chi^{(\mathrm{R})}_{xzx}\right| \\ &> 3.5\left|C^{(\mathrm{a})}(xxz)\chi^{(\mathrm{R})}_{xxz}\right|\,.\end{aligned} \tag{8}$$

Thus, $\left|C^{(\mathrm{a})}(zzz)\chi^{(\mathrm{R})}_{zzz}\right|$ is at least a few times larger than all the other components. In SFG on metal, the component of local field normal to the surface is enhanced, and the parallel component becomes smaller because of the boundary conditions of the electric field between the transparent material and metals [30, 32]. This is responsible for the large $\left|C^{(\mathrm{a})}(zzz)\chi^{(\mathrm{R})}_{zzz}\right|$ observed in the signal of SAM on metal.

3.3 Nonresonant SF signal

In contrast to the resonant SF signals, the strong nonresonant signal was observed as seen in Fig. 3c as well as in Fig. 3a,b, suggesting the non-negligible contribution of $\chi^{(\mathrm{NR})}_{xzx}$ or $\chi^{(\mathrm{NR})}_{zxx}$. Using the nonresonant SF signal intensity in Fig. 3, we can estimate the magnitude of the nonresonant components of the nonlinear susceptibility by solving the following coupled equations:

$$\begin{aligned}&\left|(C^{(\mathrm{n})}(xzx) + C^{(\mathrm{n})}(zxx))\chi^{(\mathrm{NR})}_{xzx} + C^{(\mathrm{n})}(zzz)\chi^{(\mathrm{NR})}_{zzz}\right. \\ &\left. + C^{(\mathrm{n})}(xxz)\chi^{(\mathrm{NR})}_{xxz}\right|^2 = \alpha^{(\mathrm{n})} I^{(\mathrm{n})}\,,\end{aligned} \tag{9}$$

where $I^{(\mathrm{n})}$ is the nonresonant SF signal intensity for the n configuration (n = a, b, c, d). From Fig. 3, we obtain $I^{(\mathrm{a})} = 2.9$, $I^{(\mathrm{b})} = 0.66$, $I^{(\mathrm{c})} = 1.0$, and $I^{(\mathrm{d})} = 0.26$. $\alpha^{(\mathrm{n})}$ in (9) is a factor proportional to the incident power density. By a similar calculation as made to get (8) from (7), we get from (9) the following relations for the relative magnitudes of the nonresonant components of the nonlinear susceptibility:

$$\begin{aligned}&37 < \left|\chi^{(\mathrm{NR})}_{zzz}\right| < 490, \quad 22 < \left|\chi^{(\mathrm{NR})}_{xxz}\right| < 48\,, \\ &\left|\chi^{(\mathrm{NR})}_{xzx}\right| = \left|\chi^{(\mathrm{NR})}_{zxx}\right| = 1\,,\end{aligned} \tag{10}$$

where $\left|\chi^{(\mathrm{NR})}_{xzx}\right|$ $\left(= \left|\chi^{(\mathrm{NR})}_{zxx}\right|\right)$ is normalized to unity. Using (10) and the values listed in Table 1, the nonresonant components $\left|C(ijk)\chi^{(\mathrm{NR})}_{ijk}\right|$ for the configurations (a) are estimated as follows:

$$\begin{aligned}&0.2 < \left|C^{(\mathrm{a})}(zzz)\chi^{(\mathrm{NR})}_{zzz}\right| < 2.3, \\ &0.3 < \left|C^{(\mathrm{a})}(xxz)\chi^{(\mathrm{NR})}_{xxz}\right| < 0.6\,, \\ &\left|(C^{(\mathrm{a})}(xzx) + C^{(\mathrm{a})}(zxx))\chi^{(\mathrm{NR})}_{xzx}\right| = 1\,,\end{aligned} \tag{11}$$

where $\left|(C^{(\mathrm{a})}(xzx) + C^{(\mathrm{a})}(zxx))\chi^{(\mathrm{NR})}_{xzx}\right|$ is again set to unity. Thus, all of the nonresonant components contributed to

Table 1. Calculated values of $C(ijk) \times 10^3$ for each optical configuration. $C(ijk) = e_i F^{ii} e_j F^{jj} e_k F^{kk}$, where e_i, e_j, and e_k are the corresponding i, j, and k component of the unit polarization vectors, and F^{ii} represents the i component of the Fresnel factor, respectively

(θ_{VIS}, θ_{MIR})	$C(xzx)$	$C(zxx)$	$C(zzz)$	$C(xxz)$
(a) (50°, 43°)	$4.9\,\mathrm{e}^{\mathrm{i}(120°)}$	$72\,\mathrm{e}^{\mathrm{i}(126°)}$	$0.36\,\mathrm{e}^{\mathrm{i}(-62°)}$	$1.0\,\mathrm{e}^{\mathrm{i}(117°)}$
(b) (60°, −45°)	$4.4\,\mathrm{e}^{\mathrm{i}(120°)}$	$44\,\mathrm{e}^{\mathrm{i}(125°)}$	$0.26\,\mathrm{e}^{\mathrm{i}(118°)}$	$0.83\,\mathrm{e}^{\mathrm{i}(-63°)}$
(c) (45°, 0°)	$3.8\,\mathrm{e}^{\mathrm{i}(127°)}$	$47\,\mathrm{e}^{\mathrm{i}(133°)}$	0.0	0.0
(d) (0°, 45°)	0.0	$9.4\,\mathrm{e}^{\mathrm{i}(140°)}$	0.0	$0.73\,\mathrm{e}^{\mathrm{i}(131°)}$

the nonresonant signal. This result is consistent with the second-harmonic generation (SHG) from the hexadecanethiol adsorbed on polycrystalline gold substrate [19]. Buck et al. [19] obtained $\left|\chi_{zzz}^{(\mathrm{NR})}\right| = 17.8$, $\left|\chi_{xxz}^{(\mathrm{NR})}\right| = \left|\chi_{xzx}^{(\mathrm{NR})}\right| = 7$, and $\left|\chi_{zxx}^{(\mathrm{NR})}\right| = 1$, which give $\left|C(ijk)\chi_{ijk}^{(\mathrm{NR})}\right|$ lying between 0.66 and 0.84.

The contribution of the adsorbate $\chi_{\mathrm{a}}^{(\mathrm{NR})}$ to the nonresonant part of the nonlinear susceptibility $\chi^{(\mathrm{NR})}$ is negligible, since the nonresonant signal was hardly observable for the LB film of ODT/glass. Our experimental results also show that the nonresonant signal intensity is $\approx 60\%$ of that from the clean gold substrate in the configuration (a), showing non-negligible contribution of the adsorbate–substrate interaction $\chi_{\mathrm{s-a}}^{(\mathrm{NR})}$. $\chi^{(\mathrm{NR})}$ expressed by (6) is, therefore, dominated by $\chi_{\mathrm{s}}^{(\mathrm{NR})}$ and $\chi_{\mathrm{s-a}}^{(\mathrm{NR})}$.

3.4 Interference between the resonant and nonresonant components of nonlinear polarization

In order to elucidate the interference between the resonant and nonresonant components of nonlinear polarization, the SF spectral profiles are analyzed according to the above discussions. Figure 4 shows the results obtained by fitting to the following formula [17, 32],

$$\left|P_{\mathrm{p}}^{(2)}(\omega)\right|^2 \propto \left|1+\sum_{\nu}\frac{a_\nu \mathrm{e}^{\mathrm{i}\phi}}{(\omega-\omega_\nu)/(\mathrm{i}\Gamma_\nu)+1}\right|^2, \qquad (12)$$

where a_ν and ϕ are the amplitude and phase of $C^{(\mathrm{n})}(zzz) \times \chi_{zzz,\nu}^{(\mathrm{R})}(\omega_\nu)/\sum_{i,j,k} C^{(\mathrm{n})}(ijk)\chi_{ijk}^{(\mathrm{NR})}$, the ratio of the resonant contribution at resonance to the nonresonant contribution. Here, only one resonant component, $C^{(\mathrm{n})}(zzz)\chi_{zzz,\nu}^{(\mathrm{R})}$, was considered, as has already been discussed. Within the MIR wavelength region used in the present experiment, a_ν is assumed to be independent of ω. The same values of ω_ν, Γ_ν, and the ratios among the parameters of a_ν were used for the fitting of both (a) and (b), because these are independent of the optical configuration. The obtained values are listed in Table 2. The dotted lines in Fig. 4 are the reproduction of Figs. 3a,b. The resonant frequencies are in accordance with the literature data [17, 18] within an error of a few cm^{-1}. The ratios among were determined as $a_{\mathrm{s}} : a_{\mathrm{Fer}} : a_{\mathrm{d}} \cong 1.0 : 0.8 : 1.1$, where the subscripts s, Fer, and d stand for the symmetric stretching, the overtone of the methyl deformation, and the degenerate stretching modes, respectively. We obtained $5.3\,\mathrm{cm}^{-1}$ for Γ_{s}, while Yeganeh et al. [17] reported $3.5\,\mathrm{cm}^{-1}$. This difference

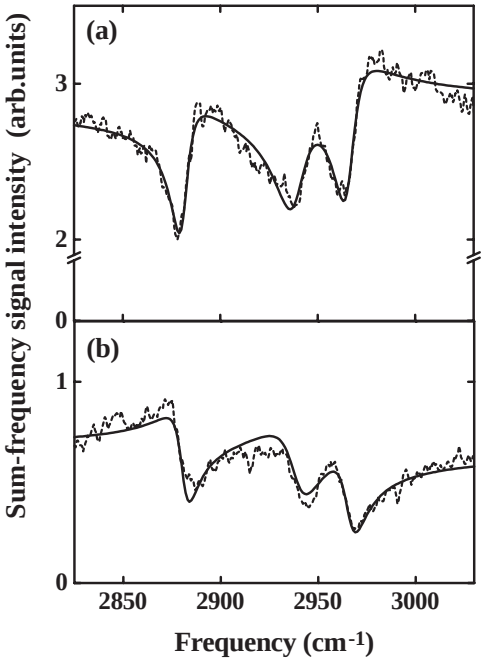

Fig. 4. The calculated SF spectral profile by using the parameters listed in Table 2 (*solid line*) and the experimental results (*dashed line*)

Table 2. Parameters used for the calculation of the SF spectral profiles in Fig. 4. (a) and (b) correspond to the co- and counter-propagating configuration as in Fig. 2. a_ν and ϕ are the amplitude and phase of the ratio of the resonant contribution at ω_ν to the nonresonant contribution

	$\omega_\nu/\mathrm{cm}^{-1}$	$\Gamma_\nu/\mathrm{cm}^{-1}$	a_ν^*	ϕ/deg.
(a) ($\theta_{\mathrm{VIS}} = 50°$, $\theta_{\mathrm{MIR}} = 43°$)				−140
1) symmetric stretching	2881	5.3	0.15	
2) Fermi resonance	2939	9.5	0.12	
3) degenerate stretching	2966	6.5	0.16	
(b) ($\theta_{\mathrm{VIS}} = 60°$, $\theta_{\mathrm{MIR}} = -45°$)				131

* The values of a_ν for the configuration (b) are 2.26 times as large as those for (a)

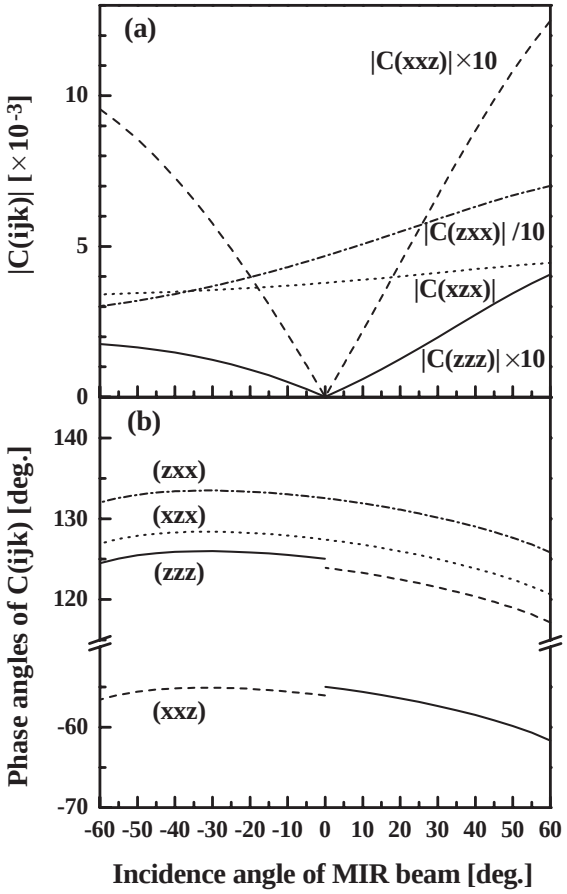

Fig. 5. Calculated amplitude (a) and phase angle (b) of $C(ijk)$ as a function of the incidence angle of the MIR beam for a fixed incidence angle of the VIS beam of 45°

in Γ_s could be due to the wide bandwidth ($\approx 10\,\mathrm{cm}^{-1}$) of the present picosecond laser compared with their laser bandwidth of $0.2\,\mathrm{cm}^{-1}$.

The angle-of-incidence dependence of ϕ can be interpreted as follows. Figure 5 shows the calculated amplitude (Fig. 5a) and the phase angle (Fig. 5b) of $C(ijk)$ as a function of the incidence angle of the MIR beam. In this calculation, the incidence angle of the VIS beam is fixed to 45°. The phase angles of each component of $C(ijk)$ shown in Fig. 5b is only weakly dependent on the MIR incidence angle as long as θ_{MIR} retains its sign, and is $\approx -55°$ for $C(xxz)$ ($\theta_{\mathrm{MIR}} < 0°$) and $C(zzz)$ ($\theta_{\mathrm{MIR}} > 0°$), and $\approx 125°$ for the others. In contrast to the weak dependence of the phase angle, $|C(zzz)|$ and $|C(xxz)|$ are strongly dependent on the incidence angles as shown in Fig. 5a. Moreover, the phase of $\chi_{ijk}^{(\mathrm{NR})}$ is generally different among the ijk components. This makes the phase angle of $\sum_{i,j,k} C(ijk)\chi_{ijk}^{(\mathrm{NR})}$ dependent on the incidence angle in a different way compared with that of the resonant contribution which is solely determined by $C(zzz)$. Thus, the difference in the angle-of-incidence dependence of ϕ arises from the fact that the nonresonant part of the nonlinear polarization is composed of the sum of all ijk components, whereas the resonant part has only zzz component. Then, the phase angle φ of $\chi_{ijk}^{(\mathrm{NR})}$ relative to $\chi_{zzz,\nu}^{(\mathrm{R})}(\omega_\nu)$ can be evaluated using the obtained values of ϕ, Table 2 and (10), as,

$$\varphi(\chi_{xzx}^{(\mathrm{NR})}) = \varphi(\chi_{zxx}^{(\mathrm{NR})}) \approx -77°, \quad \varphi(\chi_{zzz}^{(\mathrm{NR})}) \approx 175° \pm 40° . \tag{13}$$

It is to be noted that both the amplitude and phase of the nonlinear susceptibility are generally dependent on the VIS laser wavelength [19]. For the SF signal obtained by Harris et al. [18] by using the VIS laser wavelength of 532 nm in the configuration ($\theta_{\mathrm{VIS}} = 60°$, $\theta_{\mathrm{MIR}} = -60°$), the coefficients $(C(xzx) + C(zxx)) = 72.3\,\mathrm{e}^{\mathrm{i}(98°)}$, $C(zzz) = 0.80\,\mathrm{e}^{\mathrm{i}(93°)}$, and $C(xxz) = 1.7\,\mathrm{e}^{\mathrm{i}(-119°)}$ are derived by the same procedure as is described in Sect. 3.1. This gives $|\phi| > 60°$, which however cannot reproduce their phase additive SF signal corresponding to $\phi = 0°$. This would reflect a strong wavelength dependence of the nonlinear susceptibility in the visible region, which can originate from the optical resonance in gold.

4 Conclusions

The SF spectra in the various optical configurations of incident beams, for the CH vibrational modes of ODT self-assembled on gold, were found to display a profile of dispersion type due to the interference between the resonant and nonresonant contributions. Through the analysis of the SF spectral profiles, we have shown for the first time that the contribution from the zzz component of the resonant nonlinear susceptibility $\chi_{zzz}^{(\mathrm{R})}$ is dominant in the observed resonant signals. The dependence of the phase angle on the optical configuration was different between the resonant and the nonresonant contributions of the nonlinear polarization, because the phase angle for the nonresonant part of the nonlinear polarization is composed of the sum of all ijk components whereas only zzz component for the resonant part.

Acknowledgements. The authors are grateful to Dr. K. Kajikawa and Mr. M. Mihara for their helpful suggestions and technical help.

References

1. J.H. Hunt, P. Guyot-Sionnest, Y.R. Shen: Chem. Phys. Lett. **133**, 189 (1987)
2. K. Wolfrum, H. Graener, A. Laubereau: Chem. Phys. Lett. **213**, 41 (1993)
3. R.P. Chin, J.Y. Huang, Y.R. Shen, T.J. Chuang, H. Seki, M. Buck: Phys. Rev. B **45**, 1522 (1992)
4. N. Akamatsu, K. Domen, C. Hirose, T. Onishi, H. Shimizu, K. Masutani: Chem. Phys. Lett. **181**, 175 (1991)
5. N. Akamatsu, K. Domen, C. Hirose: J. Phys. Chem. **97**, 10070 (1993)
6. Y.R. Shen: Surf. Sci. **299**/**300**, 551 (1994)
7. Y. Goto, N. Akamatsu, K. Domen, C. Hirose: J. Phys. Chem. **99**, 4086 (1995)
8. P. Guyot-Sionnest, J.H. Hunt, Y.R. Shen: Phys. Rev. Lett. **59**, 1597 (1987)
9. K. Wolfrum, A. Laubereau: Chem. Phys. Lett. **228**, 83 (1994)
10. K. Wolfrum, J. Lobau, A. Laubereau: Appl. Phys. A **59**, 605 (1994)
11. Q. Du, X.-d. Xiao, D. Charych, F. Wolf, P. Frantz, Y.R. Shen, M. Salmeron: Phys. Rev. B **51**, 7456 (1995)
12. A.L. Harris, N.J. Levinos: J. Chem. Phys. **90**, 3878 (1989)
13. A.L. Harris, L. Rothberg, L.H. Dubois, N.J. Levinos, L. Dhar: Phys. Rev. Lett. **64**, 2086 (1990)
14. A.L. Harris, L. Rothberg, L. Dhar, N.J. Levinos, L.H. Dubois: J. Chem. Phys. **94**, 2438 (1991)
15. M. Morin, N.J. Levinos, A.L. Harris: J. Chem. Phys. **96**, 3950 (1992)
16. K. Kuhnke, M. Morin, P. Jakob, N.J. Levinos, Y.J. Chabal, A.L. Harris: J. Chem. Phys. **99**, 6114 (1993)
17. M.S. Yeganeh, S.M. Dougal, R.S. Polizzotti, P. Rabinowitz: Phys. Rev. Lett. **74**, 1811 (1995)
18. A.L. Harris, C.E.D. Chidsey, N.J. Levinos, D.N. Loiacono: Chem. Phys. Lett. **141**, 350 (1987)
19. M. Buck, F. Eisert, M. Grunze, F. Träger: Appl. Phys. A **60**, 1 (1995)
20. R. Superfine, J.Y. Huang, Y.R. Shen: Chem. Phys. Lett. **172**, 303 (1990)
21. R. Superfine, J.Y. Huang, Y.R. Shen: Opt. Lett. **15**, 1276 (1990)
22. X.D. Zhu, W. Daum, X.D. Xiao, R. Chin, Y.R. Shen: Phys. Rev. B **43**, 11571 (1991)
23. A. Ulman: *An Introduction to Ultrathin Organic Films From Langmuir–Blodgett to Self-Assembly* (Academic Press, New York 1991) and references cited therein
24. S. Lin, Y. Tanaka, M. Aono, T. Suzuki: Jpn. J. Appl. Phys. **36**, 3510 (1997)
25. H. Ohde, S. Lin, A. Minoh, F.O. Shimizu, M. Aono, T. Suzuki: Appl. Phys. B **62**, 15 (1996)
26. Y.R. Shen: *The Principles of Nonlinear Optics* (Wiley, NewYork 1984)
27. T.F. Heinz: *Nonlinear Surface Electromagnetic Phenomena*, ed. by H.-E. Ponath, G.I. Stegeman (North-Holland, Amsterdam 1991) pp. 353–416
28. C. Kittel: *Introduction to Solid State Physics* (Wiley, New York 1968) Chap. 12
29. V. Mizrahi, J.E. Sipe: J. Opt. Soc. Am. B **5**, 660 (1988)
30. R. Superfine, P. Guyot-Sinnest, J.H. Hunt, C.T. Kao, Y.R. Shen: Surf. Sci. **200**, L445 (1988)
31. D.W. Lynch, W.R. Hunter: *Handbook of Optical Constants of Solids*, ed. by E.D. Palik (Academic Press, New York 1985) pp. 275–295
32. J. Miragliotta, R.S. Polizzotti, P. Rabinowitz, S.D. Cameron, R.B. Hall: Chem. Phys. **143**, 123 (1990)